SCANNING STRATEGIES IN ELECTRON BEAM MELTING TO INFLUENCE MICROSTRUCTURE DEVELOPMENT

Diego Bermudez[*], Cesar A. Terrazas[*], Philip Morton[*], and Ryan Wicker[*]

*The University of Texas at El Paso, W.M. Keck Center for 3D Innovation, El Paso, TX, USA, 79968

Abstract

Recent advances with the use of electron beam melting (EBM) additive manufacturing (AM) have indicated the ability to control the resultant microstructure based on control of the processing parameters. An Arcam A2 EBM system was utilized to control the size of the microstructure for Ti-6Al-4V components. The methodology employed allowed to refine the microstructure at selected regions of a part while maintaining a more typical acicular α+β microstructure in the rest of the components. This process was achieved by partitioning the layer data into two files that enabled different scanning conditions during fabrication. The first scan consisted of hatching of the component geometry (circle with dimensions of 15mm in diameter) excluding a center circle with dimensions of 1mm in diameter. Following the first scan, a point-wise melting for the center circle was completed. The strategy generated a finer structure in the center circle in comparison with the more regular sized microstructure in the rest of the build. Components built were sectioned and prepared into metallographic specimens that were observed through optical microscopy. The micrographs were used to measure the length and width of alpha laths.

Introduction

Additive manufacturing (AM) methods have gained relevance in the past few years since they enable the fabrication of high complexity, high value components, often at reduced lead times. The electron beam melting (EBM) process is a powder bed fusion AM technology that uses a high-power electron beam as a source to selectively preheat and melt metal powders. The throughput achieved by EBM, when compared to other AM processes, and the ability to process highly reactive materials including titanium alloys has generated interest for industries that include aerospace, automotive, and medical.

Ti-6Al-4V is a two-phase alloy that forms an α-phase that grows from β during solidification. Aluminum is a stabilizer that helps make the compound light weight, while vanadium acts as a β stabilizer that provides ductility. The alloy is the material with the most development for the EBM process since the commercial introduction of the technology in 2003 (Ljungblad, 2016). With mechanical characteristics that fall between those of aluminum and iron, some of the alloy's highly desirable properties include a light strength-to-weight ratio, and high corrosion and temperature resistance. Typically, a duplex Widmanstatten microstructure is obtained for Ti-6Al-4V processed by EBM. This microstructure forms by a diffusion controlled nucleation and growth process. The size of the microstructure is highly dependent on the cooling rate. While slower cooling rates yield thicker alpha and longer alpha laths, faster cooling rates promote thinner and shorter laths (Azani, 2016). In previous research, it has been demonstrated that the modification of the standard fabrication parameters in EBM is an effective method to influence the microstructural and mechanical performance. For instance, using thermography information from an infrared (IR) camera, researchers were able to influence the fabrication temperature profile for various builds and, more importantly, to tailor the microstructure by

controlling the energy input through tuning of the fabrication parameters (Mireles *et al.*, 2015). In a similar study, fatigue life performance was improved for an EBM fabricated Ti-6Al-4V bracket by promoting microstructure coarsening through the use of additional melt scan sequences (Morton *et al.*, 2015). Building upon the results from these previous studies, in this research a technique was developed and implemented where different melt scans were applied to discrete regions of the build, selectively influencing the development of microstructures. In particular, the microstructure of a region within a component was refined. The results were confirmed by optical microscopy observations and measurements of the length and width of alpha laths. These results further confirm the ability to selectively refine the microstructure during EBM processing of Ti-6Al-4V.

Methodology

Electron Beam Melting

An Arcam A2 (Arcam AB, Sweden) machine was used for this study. Arcam's EBM process employs a high energy electron beam (3.5 kW) to preheat and melt metal powders. The fabrication process takes place at an elevated bed temperature of approximately 730°C to reduce residual stresses. For Ti-6Al-4V, the process is performed under a controlled vacuum environment (pressure of 2.0^{-3} mBar) by a constant helium bleed that prevents oxidation of the feedstock material. A stainless-steel plate is used as a substrate to begin fabrication. Figure 1 shows the schematic of the Arcam A2 system listing all major components.

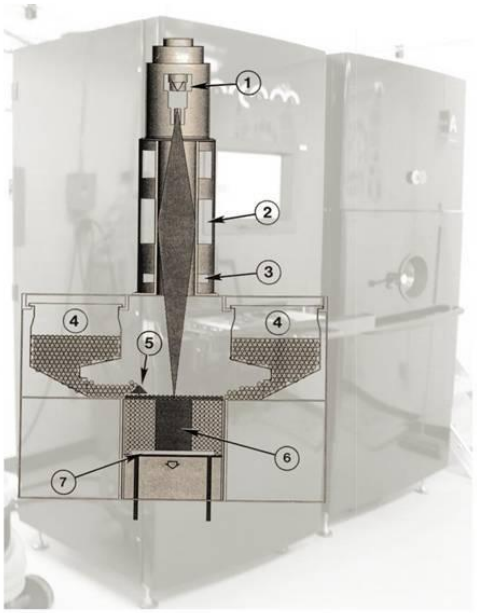

Figure 1. Schematic of inside arrangement of the Arcam_A2 system showing key components: (1) Electron gun assembly; (2) Electron Beam focusing lens; (3) Electron Beam deflection coils; (4) Powder cassettes; (5) Powder rake; (6) Build specimen; (7) Build stage. After (Murr *et al.*, 2009).

Material.

For this study, the Ti-6Al-4V powder was purchased from Arcam. Powder had the recommended size distribution of 45-106μm. The production of parts was completed using standard Arcam parameters for Ti-6Al-4V for layer thicknesses of 50μm.

Part design and fabrication

A total of nine parts were built in the experiment for this study. The parts were designed as cylindrical components with overall dimensions of 16mm in diameter by 25mm in height. A number of circular holes were extruded along the longitudinal axis of the cylinders. The parts were separated into three groups based on the number of extruded holes running throughout their height (Figure 2). The solid cylinders (Group N) served as baseline to compare microstructure, whereas cylinders having one extruded hole, and seven extruded holes, were assigned to Group P and Group M respectively. For each of the builds in both Group P and Group M, the extruded holes had a diameter of ~1mm. Separate models consisting of a single or multiple extruded rods (measuring ~1mm in diameter) were also designed in CAD. For this work, the models of the rods were made to fit and overlap inside the extruded holes of the cylinders. Using this approach, the scanning strategy was influenced for these models during EBM fabrication.

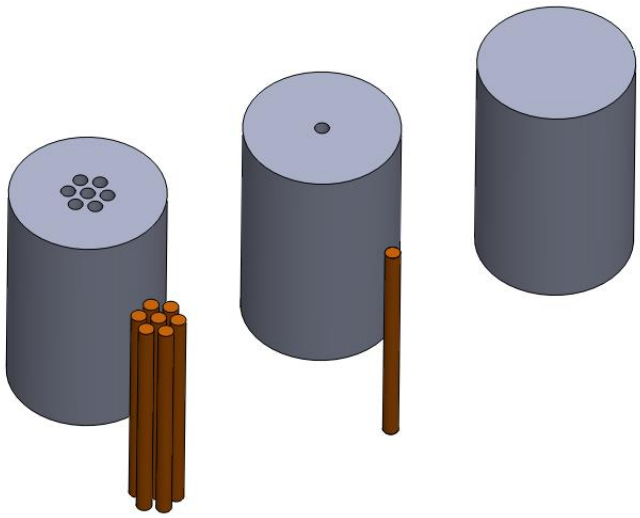

Figure 2. Schematic showing the CAD of the parts built in this study.

Melt Scan Strategy

The regular sequence of steps in EBM includes preheating of the powder bed, followed by melting of contours and hatch area through vector scanning of the surface as indicated from the digital file. In this work, this melt scan strategy was controlled by the use of the different CAD models as described before; as indicated by Figure 3, the surface for each component (blue hatch) was vector scanned using the electron beam, whereas for the remaining surfaces (orange dots) point-wise melting was effectively achieved. Recalling the discussion from the previous section,

the orange dots corresponded to the surface of the rods created as the second CAD models created. This scanning strategy was performed for every layer during fabrication of the components. It was hypothesized that the point-wise melting of the orange regions resulted in higher cooling rates leading to refined microstructure. Previously, refined microstructures were observed in EBM fabricated Ti-6Al-4V thin walls (~1mm thick) or single melt pool track (Murr *et al.*, 2010, Tan *et al.*, 2016)

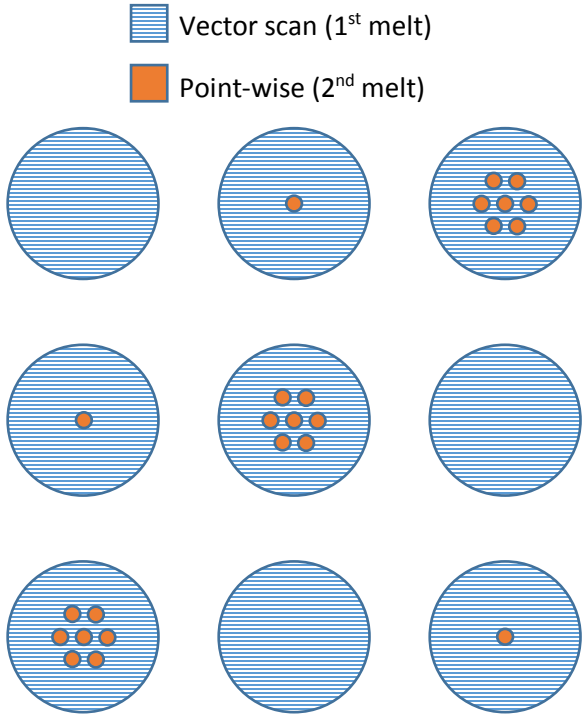

Figure 3. Melt scan strategy implemented.

Metallography and Microscopy

Microscopy characterization was performed using an optical microscope (Reichert MEF4 A/M Inverted metallographic system) to confirm the variance of microstructural dimensions that would indicate differences in solidification rates. All nine fabricated parts were segmented at two planes and mounted in resin for metallographic preparation, as shown in Figure 4. To evaluate the ability to maintain the microstructure refinement throughout the height of components, two sections were obtained from each component and denoted Plane A and Plane B respectively, as also shown in Figure 4.

The metallographic preparation consisted of grinding the mid-plane surface by progressively increasing grinding paper grit size from 220 to 1200, and finally polishing the surface using a polishing pad and fine alumina powder solutions of sizes 0.3μm, 0.1μm, and 0.05μm in that order. To reveal the microstructure under the microscope, a modified Kroll's Reagent solution consisting of 92 mL of distilled water (H_2O), 6 mL of nitric acid (HNO_3), and 2 mL of hydrofluoric acid (HF) was prepared and applied on the polished surface. The etching procedure on the samples consisted of dipping the sample into the fresh Kroll's solution for approximately 15 seconds and immediately rinsing with distilled water. The three specimens

produced from each group were sectioned and prepared for microstructure observations. This allowed to compare the microstructure size differences amongst specimens having either a single or multiple point-wise melt regions. Specimens without point-wise melting were used as controls.

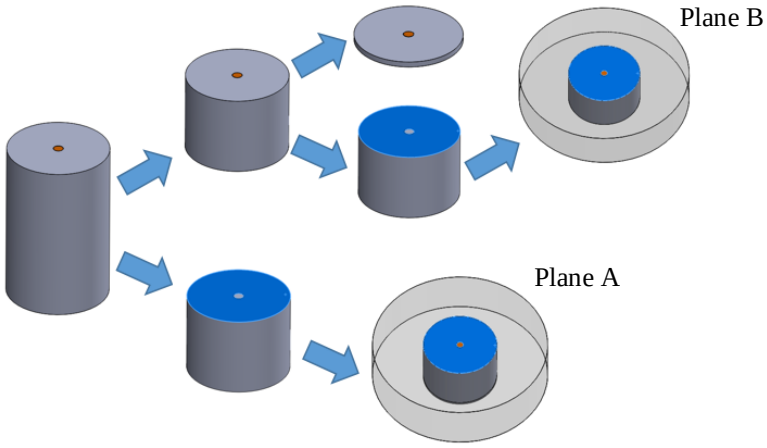

Figure 4. Representative sectioning of a part. The blue shading indicates the analyzed face for each of the nine parts. Two metallographic specimens were produced from each sectioned component denoted as Plane A and Plane B.

Three regions of interest (Figure 5) were captured in micrographs at 50x magnification for comparative analysis using a digital camera (AM Scope 3MP Microscope Digital Camera). The first region (R1) denotes areas of the specimen that were processed by point-wise melting, the second region (R2) indicates the area that was vector scanned, and the third region (R3) shows the interface area where a transition in microstructure was observed. Micrographs obtained for regions R1 and R2 allowed to obtain width and length measurements of the alpha laths as described next.

Microstructure Colony Selection

The micrographs obtained were used to measure and capture the dimensions of individual alpha laths. For each micrograph, ten colonies of the alpha-beta microstructure were selected at random and the alpha laths measured. For the Ti-6Al-4V and other titanium alloys, colonies are considered as groups of aligned, alternating alpha and beta lamellae that nucleate and grow together in the same direction during solidification (Chan, 1981). The micrographs obtained show the alpha lamellae (light contrast) and the beta prior grains (dark contrast). After the selection of the colonies, individual measurements were taken. Due to the random size of colonies, measurements varied per colony, but no less than 10 measurements were captured in each. Figure 6a schematically shows the selection of ten randomly occurring colonies within an obtained micrograph. Specifically, this corresponds to the region R2 from a specimen belonging to Group N. This measurement process

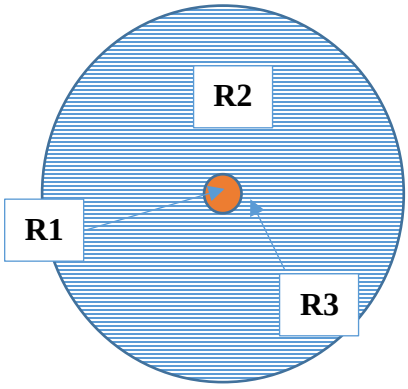

Figure 5. Schematic of regions selected for microstructural observation.

was straightforward for the microstructure in regions R2 of the various specimens as the alpha-beta laths could be easily identified.

For the case of the micrographs obtained of the refined regions (R1), a slightly different approach was used to measure the alpha laths. This was necessary since the size of the alpha laths in this region was smaller and the features more difficult to detect. Furthermore, the development of colonies (as those seen in Figure 6a) was not readily apparent in these micrographs. For these micrographs, ten random regions were selected and measurements taken for all the R1 regions of the various specimens. Figure 6b shows a characteristic micrograph of an R1 region for one of the specimens in Group P.

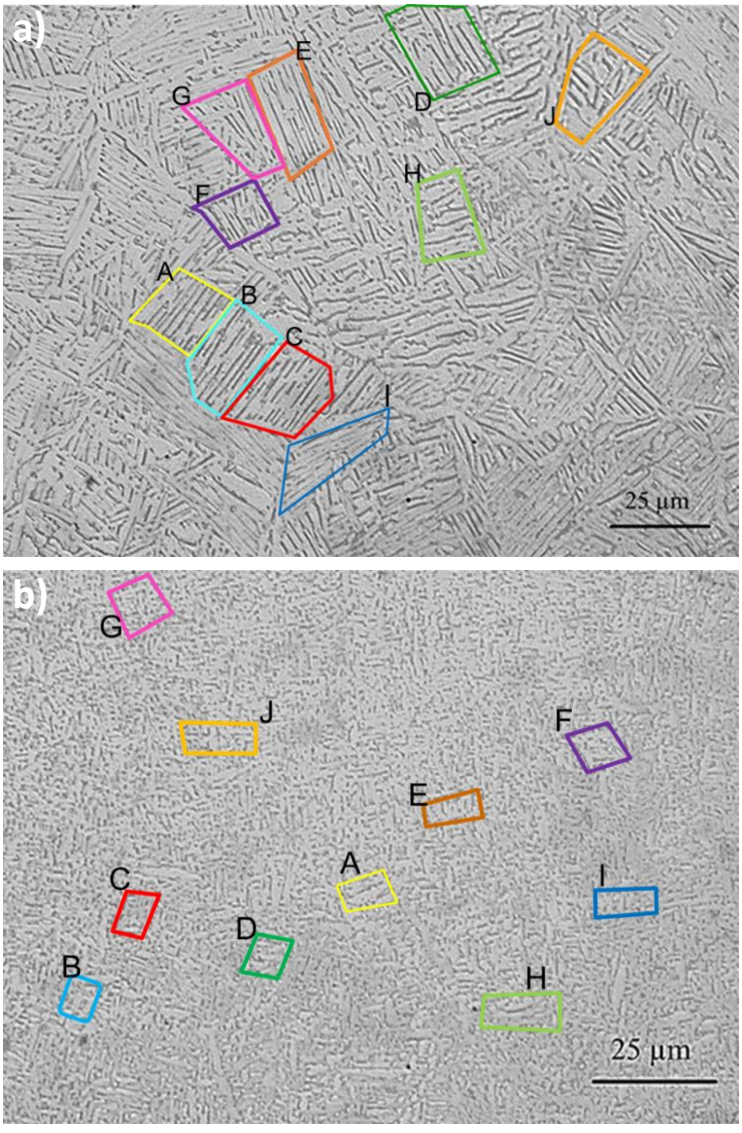

Figure 6. Selection of random alpha-beta colonies from a micrograph corresponding to a) region R2 of a Group N specimen and b) R1 of specimen from Group P.

Alpha Laths Measurements

Dimensions of width and length were made on the alpha laths by using the image analysis software Image J. First, Image J was used to convert a JPG image into a binary image. After opening the image with the software, a threshold adjustment was performed to contrast the phases and convert to binary image. The scale in the micrograph was used as the reference to obtain length and width measurements. This process allowed discerning between the alpha and beta phases given their contrast in the binary image. Accurately delineating the phases simplified taking precise measurements for the lengths and widths of alpha laths. Within ImageJ measurements were taken by tracing a line in between two dark lines (representing the boundaries of alpha laths), either in the width or length directions (Figure 7). Upon selecting a colony, the thickness and length for all alpha laths within the colony were measured. After measuring the laths in a colony, the values were averaged, the standard deviation was determined. The calculated values were taken as representatives for each specimen analyzed. This process was repeated for all selected colonies successively until all ten colonies in one micrograph were accounted for. Overall, 18 micrographs were employed to take measurements. Three micrographs were used to measure the alpha laths width and length for regions R1 and R2 for each specimen in Groups M, N and P.

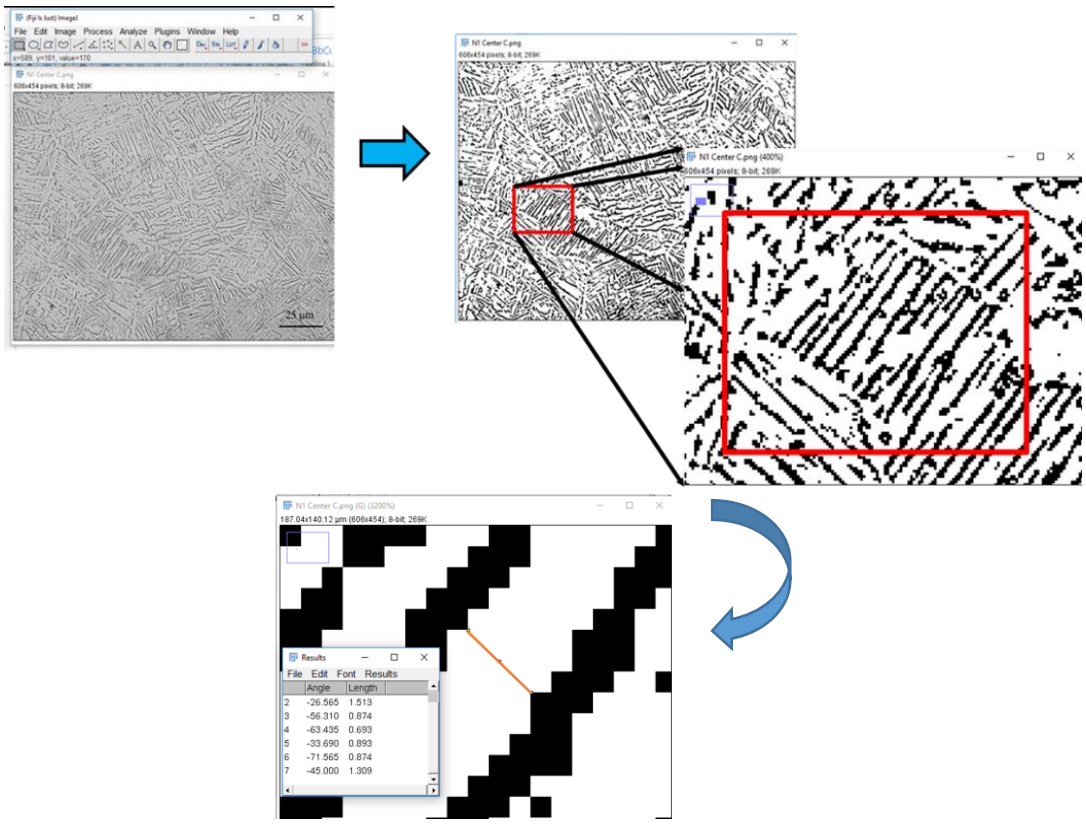

Figure 7. Process employed in ImageJ software to convert micrograph into binary image and to perform measurements. The image shows this for the width.

Results

Microscopy

The metallographic analysis confirmed the variance in the microstructure from regions that were vector scanned versus those that were created with the point-wise melting strategy. Group N served as the baseline to evaluate microstructural variations since this group had no regions that were melted through the point-wise melt strategy. For the components in this group, the microstructure from all three regions showed no measurable difference. Micrographs showing the representative microstructure for a specimen belonging to Group N, for all three regions of interest are shown in Figure 8. In all cases, the microstructure corresponds to a duplex microstructure consisting colonies of α laths within prior β grains.

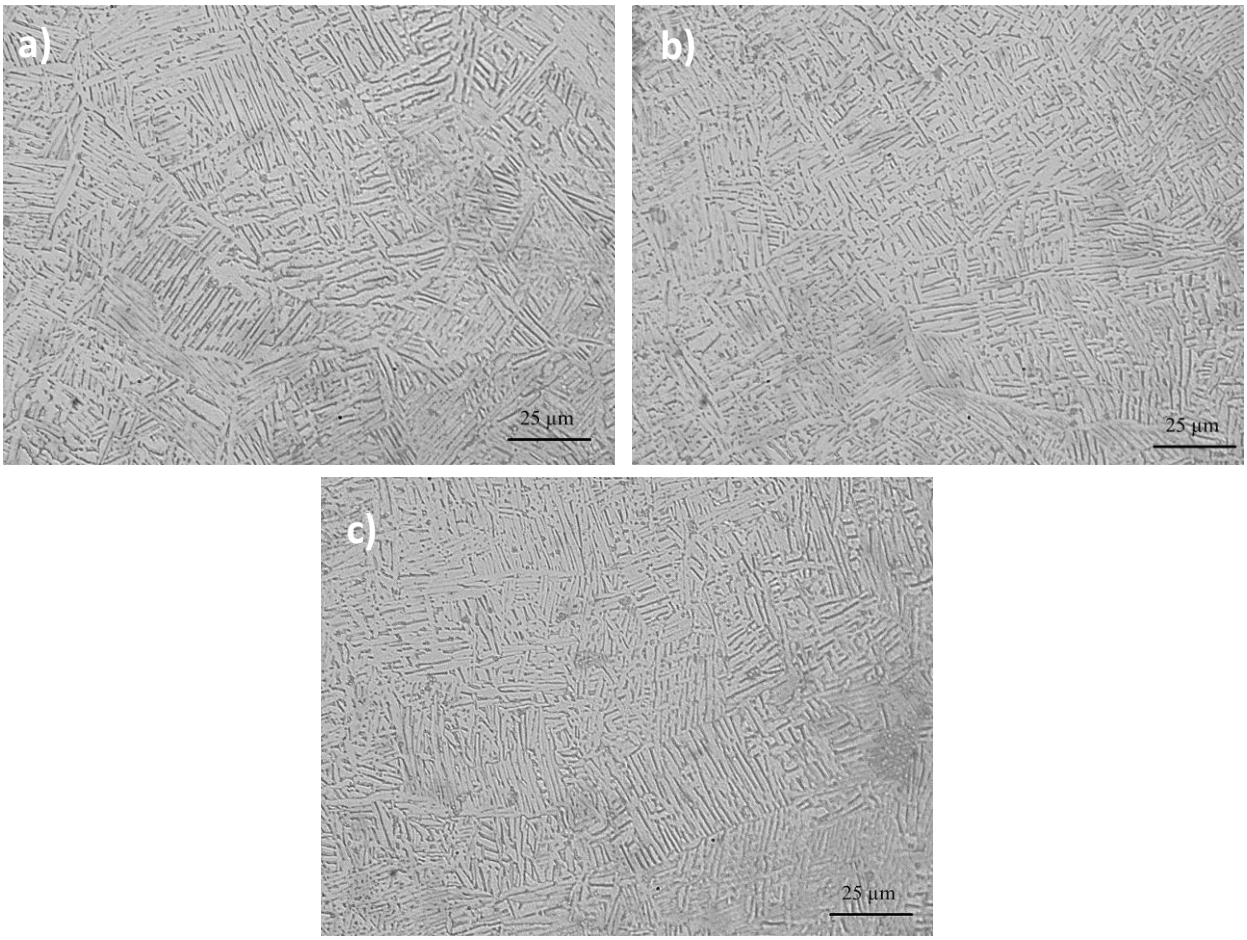

Figure 8. Micrographs obtained for regions a) R1, b) R2, and c) R3 for a representative specimen from Group N.

For specimens assigned to Group P, a sharp contrast was observed between the microstructure present in the vector scanned region versus the point-wise melted region. The reduced length in the length and width of the α laths is evident the micrograph shown in Figure 9a). Part a) of the figure corresponds to region R1, which was processed through point-wise melting. In contrast, part b) of the figure shows the representative microstructure for region R2,

that was processed using the regular vector hatching technique. Part c) of the figure corresponds to the micrograph of region R3, arguably representing the interface between refined (R1) and regular (R2) microstructures. In this micrograph, the refined microstructure is shown towards the bottom left corner while the regular microstructure is more prevalent in the rest of the image.

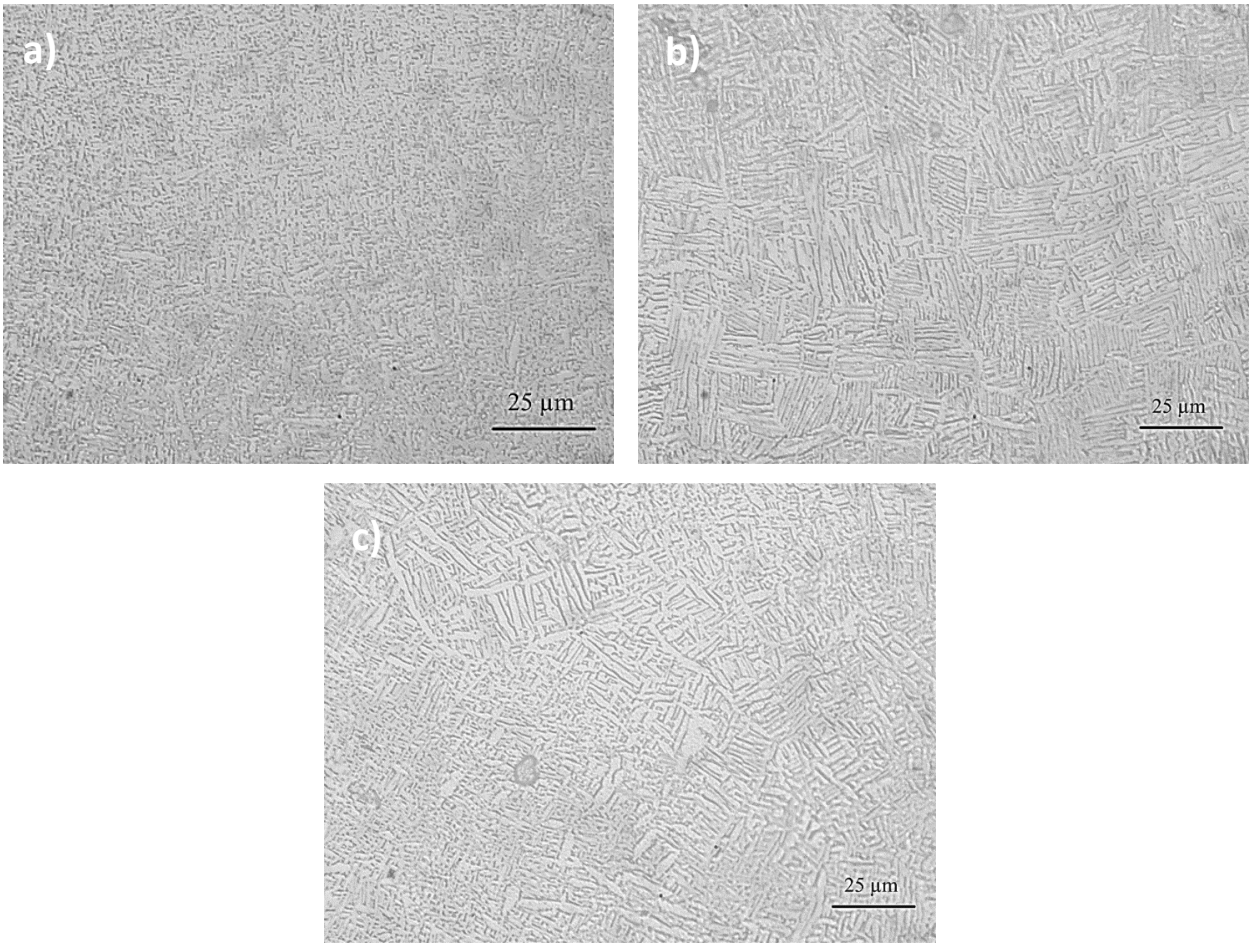

Figure 9. Micrographs obtained for regions a) R1, b) R2, and c) R3 for a representative specimen from Group P. Refined microstructure is observed for R1 versus R2.

For specimens in Group M, a lesser effect in the refinement of microstructure was observed for region R1 versus R2 and R3. The refinement of the alpha laths appears to be reduced in these micrographs as opposed to those shown in specimens belonging to Group P. This might be explained due to the multiple melt-point areas processed in these specimens as opposed to the ones belonging to Group P. Figure 10 shows the micrographs for a) region R1, b) region R2, and c) region R3. In all instances, the microstructure observed corresponds again to the duplex microstructure of α laths within prior β grains. Comparatively, micrograph a) of the figure shows α laths with smaller widths and lengths, when compared to micrographs b) and c).

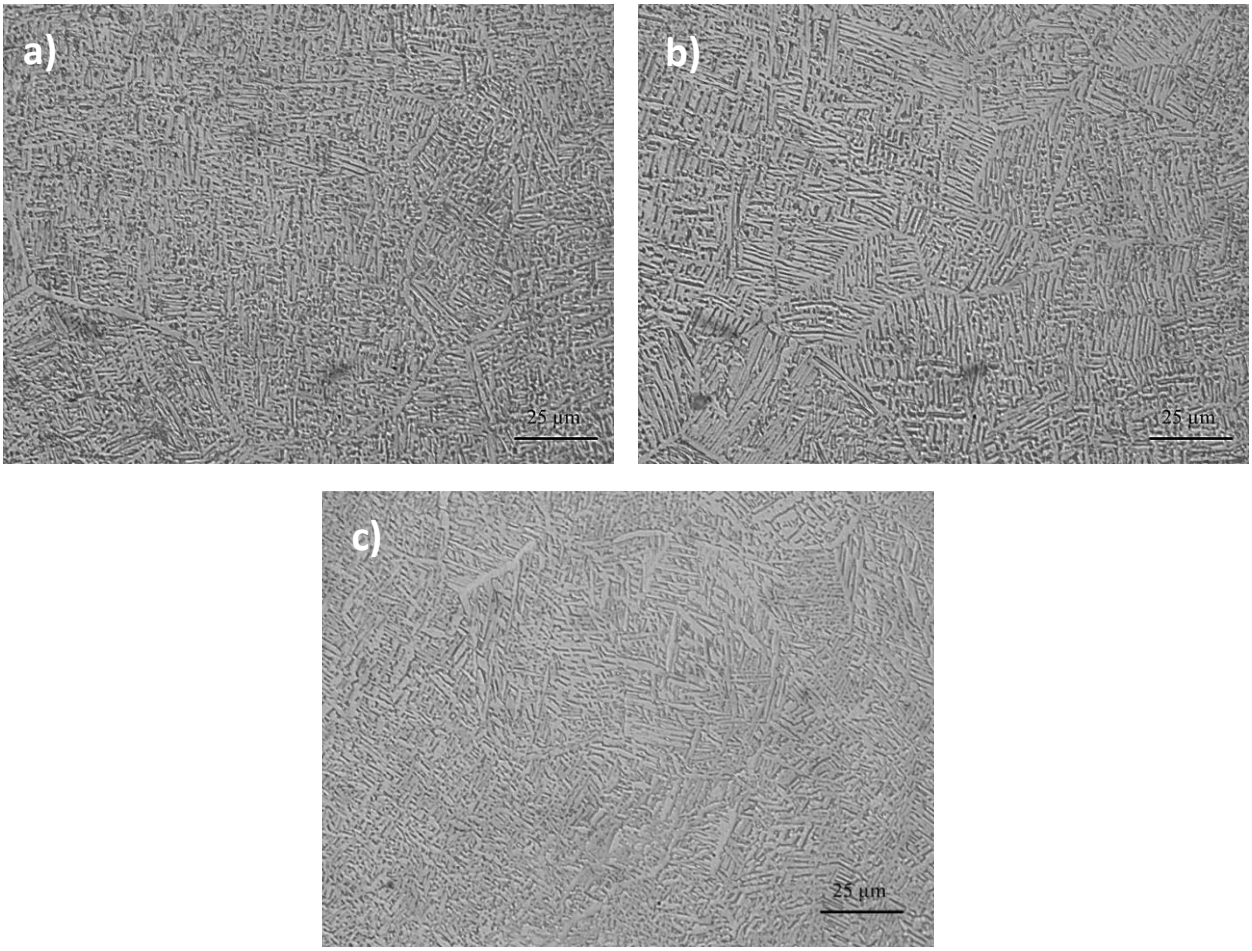

Figure 10. Micrographs obtained for regions a) R1, b) R2, and c) R3 for a representative specimen from Group M. Image a) shows refined α laths when compared to b) or c), but effect is less pronounced than for specimens in Group P.

Refined microstructure along specimen height

Consistency in microstructure variation was demonstrated along the height for one coupon selected for analysis. The coupon selected for this analysis was one belonging to the Group P. To perform this analysis, the part was cut at two planes (denoted as A and B). Measurements were taken for regions R1 andR2 for the two planes. The results are summarized graphically in Figure 11. Images a) and c) correspond to the refined microstructure observed in region R1 for planes A, and B respectively. Parts b) and d) show the characteristic microstructure of R2 for the two planes. Figure 12 shows a bar chart with the results for the average measured dimensions (width and length) of regions R1 and R2 for the two planes studied.

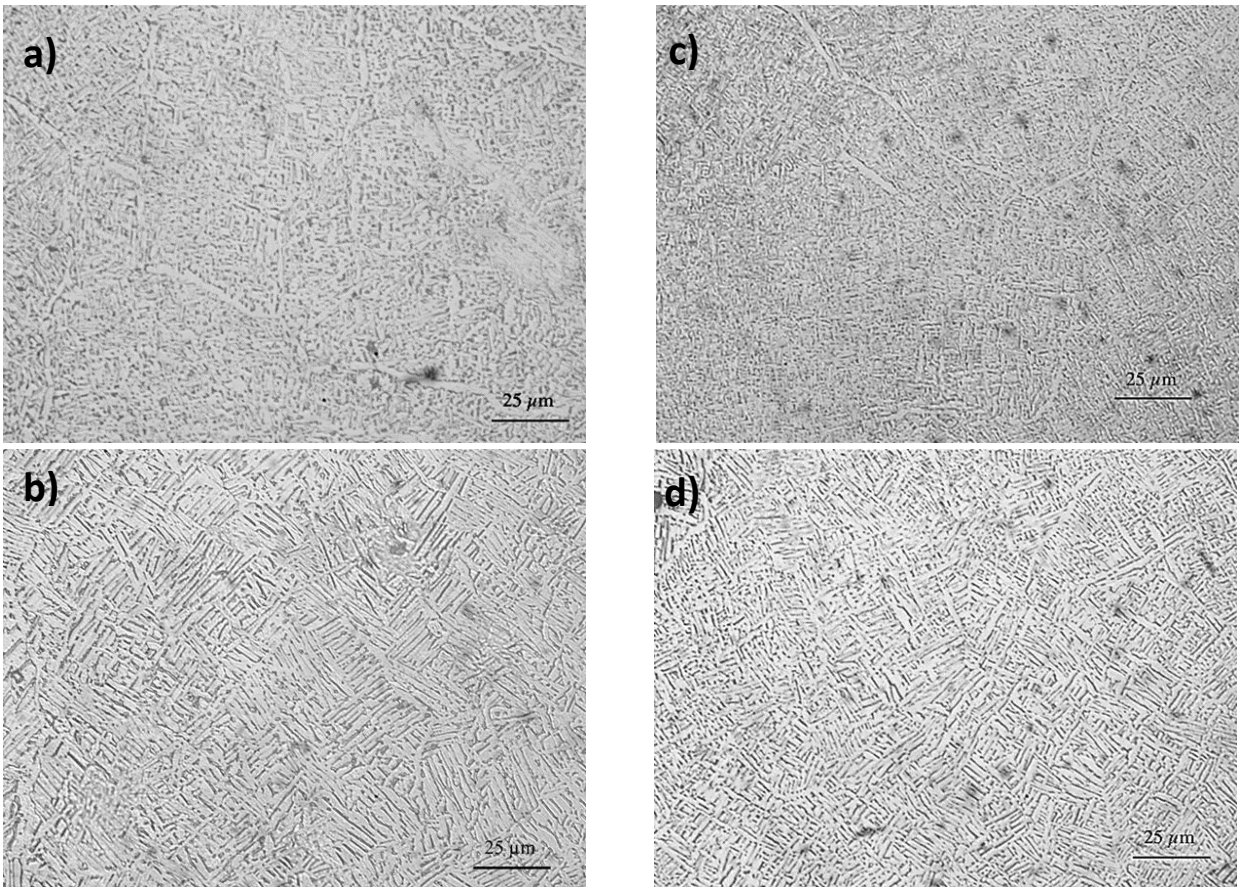

Figure 11. Micrographs obtained of two sections from one Group P part. Plane A micrographs are a) R1 and b) R2. Plane B micrographs are d) R1 and e) R2. Ability to maintain microstructural refinement along build's height is confirmed.

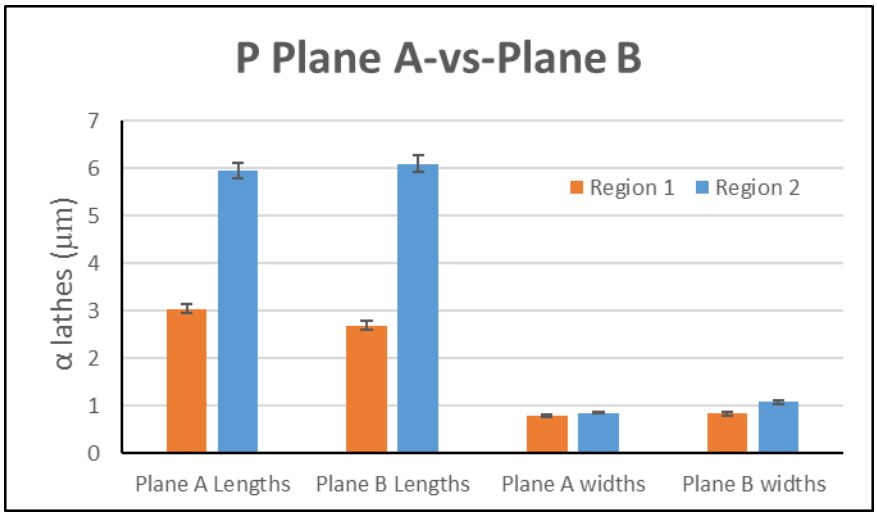

Figure 12. Lengths and widths of planes A and B comparing regions R1 and R2. In both planes analyzed, a sharp drop between regions R2 (blue) and R1 (orange) is observed.

The sharp drops in length dimensions across regions are consistent on both planes, with a higher average value of length in R2 than in the point wise melt region R1. Width average values also saw a decrease from R2 to R1, though they do not vary as much as the average length values.

Average values of measurements

The averaged measurements of values of α lengths and α widths from the colonies in the micrographs quantitatively confirm the microstructural variance between the vector scanned regions R2 and the point wise melt regions R1. The average values and standard deviation obtained for all Groups M, N, and P, are condensed and segregated on Figure 13 as α lengths and α widths from regions R1 and R2 for each. It can be seen that little variation is present in Group N values since these are the baseline for comparison of Groups M and P. Length average values show variance with Group P samples; width average values of Group P show a slight variance than the length values. Group M length values also see drops in their averages, but to a lesser extent than those values in Group P parts.

Lengths				
	Region 1	Region 2	StdDev R1	StdDev R2
N1	5.8	5.8	2.4	2.5
N2	7.3	5.9	3.6	2.8
N3	5.4	6.1	3.0	2.7
P1	3.0	6.0	1.4	2.9
P2	2.5	5.5	1.1	2.5
P3	2.4	4.3	1.1	2.4
M1	3.2	5.3	1.5	2.5
M2	3.1	3.7	1.4	2.4
M3	3.3	4.4	1.5	2.6

Widths				
	Region 1	Region 2	StdDev R1	StdDev R2
N1	0.91	0.84	0.29	0.33
N2	0.94	0.98	0.35	0.37
N3	0.89	0.74	0.37	0.27
P1	0.79	0.85	0.31	0.33
P2	0.61	0.83	0.19	0.31
P3	0.59	0.69	0.21	0.22
M1	0.66	0.84	0.27	0.27
M2	0.67	0.74	0.26	0.31
M3	0.62	0.68	0.23	0.22

Figure 13. Average values of the micrographs from Regions R1 and R2 for each specimen fabricated. On the left, α-laths length averages are displayed, and the α width averages are displayed on the right.

Discussion

A variation of duplex microstructure (α+β grains) was observed generally throughout the samples evaluated. Alpha lath dimensional averages and their morphology differed depending on which group and which regions were analyzed, as well as the scanning strategy implemented. Group N parts were fabricated as solid cylinders to serve as a baseline for microstructural comparison since they experienced a traditional EBM scanning that allowed for a conventional solidification process of the component, resulting in a structure conformed of a visibly predominant lamellar colony structure with scattered zones containing Widmanstätten (or basket weave) arrangement. The parts in Group N exhibited a continuity of lamellar microstructure independently of whether the images analyzed were from region R1 or region R2, this result was consistent as no regions were processed by point wise melting. Parts from Group P experienced the most prominent microstructural variance between vector scan strategy region R2 and point wise melt regions R1; measurements of individual α laths measurements showed sharp differences in length between R2 and R1, with smaller dimensions averaging at the point wise melt region.

Width dimensions also resulted in refinement in the point wise melt region, although the variance is far less notable. Group M parts had the same effect of laths refinement in region R1 like Group P parts, except α length differences were not developed at such a large extent as in the case of Group P probably due to the multiple point-melts in this group, as opposed to Group P. All parts fabricated exhibited a traditional Widmanstätten morphology of alpha and beta grains and lamellar colonies in region R2. Parts with point wise melt scan strategy, such as from groups P and M revealed quantifiable reduced dimensions of the α laths.

The ability to maintain continuity of refinement along the height of the build analyzed is supported by the observations performed at two planes (A, and B) of a Group P part. The similar values of the microstructural sizes for alpha laths in both planes support the hypothesis that control of the microstructure can be achieved along the build direction, although these results stem from only one build analyzed, so further scrutiny of this effect must be netted from other parts in the study.

Conclusions

Dual scanning strategies, regular vector scan melting and point wise melting, were implemented for the fabrication of Ti-6Al-4V components using an Arcam A2 machine. The components resulted in microstructural variations. The dimensions of the α-laths (width and length) were measured using image analysis software. The measured values for microstructural features confirmed regions of refined microstructure at locations within the components that were processed through point wise melting. Further research will be performed to obtain mechanical properties, including hardness and tensile testing of components with this dual size microstructure. Also, other characterization techniques will be employed to further identify the phases that develop through the scanning process employed in this work.

References

Azani, Paola. Effects of fabrication conditions on mechanical properties of Ti-6Al-4V fabricated by powder bed fusion additive manufacturing. Diss. THE UNIVERSITY OF TEXAS AT EL PASO, 2016.

Gaytan Guillen, Sara Marisela. *Additive layer manufacturing of Ti-6Al-4V by electron beam melting from powder particles: Solid, mesh and foam components study*. THE UNIVERSITY OF TEXAS AT EL PASO, 2009.

Mireles, J., Terrazas, C., Gaytan, S. M., Roberson, D. A., & Wicker, R. B. (2015). Closed-loop automatic feedback control in electron beam melting. *International Journal of Advanced Manufacturing Technology*, 78(5–8), 1193–1199.

Ljungblad U. (2016). Presentation: History and Future of EBM. EBAM 2016, Nuremberg, Germany.

Campbell, F. C., and Flake C. Campbell. "Titaium/ Alpha-Beta Alloys." Elements of Metallurgy and Engineering Alloys. N.p.: n.p., 2008. 532-34. Print.

Murr, L. E., Quinones, S. A., Gaytan, S. M., Lopez, M. I., Rodela, A., Martinez, E. Y., … Wicker, R. B. (2009). Review article Microstructure and mechanical behavior of Ti – 6Al – 4V produced by rapid-layer manufacturing , for biomedical applications, *2*(1), 20–32.

] Blackmore, M. L., Zhang, W., & Todd, I. (2010). The Origin of Microstructural Diversity , Texture , and Mechanical Properties in Electron Beam Melted Ti-6Al-4V.

Chan, K. S., Wojcik, C. C., & Koss, D. A. (1981). Deformation of an alloy with a lamellar microstructure: experimental behavior of individual widmanstatten colonies of an α-β titanium alloy. *Metallurgical Transactions A*, *12*(11), 1899–1907. https://doi.org/10.1007/BF02643801